


Cite this: *RSC Adv.*, 2017, 7, 50928

Preparation and characterization of Co and Ga₂O₃-codoped ZnS and ZnSe bulk ceramics

Yong Pan,  Li Wang,* ShuFeng Li, DongWen Gao and XiaoWei Han

The bulk ceramics (Co)_x(Ga₂O₃)_{0.6-x}(ZnS/Se)_{0.4} ($x = 0.1, 0.3$ and 0.5) were fabricated *via* a solid state reaction in a high temperature pipe boiler at temperatures ranging from 1000 to 1400 °C. The structure, optical, valence and morphological properties were determined by XRD, XPS, Raman spectroscopy, SEM, UV-vis spectroscopy and IR absorption spectroscopy. The impressive effect of the sintering temperature on the doping elements was investigated, and the optimum sintering temperature in the range 1000–1200 °C was revealed, by analysis of the mass loss, molar ratio and shrinkage rate of (Co)_x(Ga₂O₃)_{0.6-x}(ZnS/Se)_{0.4}. The zinc-blende structure of the bulk ceramic, and optimum doping ratio of (Co)_{0.5}(Ga₂O₃)_{0.1}(ZnS/Se)_{0.4}, was confirmed by XRD and Raman spectroscopy. A broad and continuous absorption band from visible to infrared wavelengths was demonstrated for (Co)_{0.5}(Ga₂O₃)_{0.1}(ZnS/Se)_{0.4}. The +2 and +3 valences of Co and Ga in the materials was proved by XPS. The surface morphology of the films was visualised by SEM and exhibited excellence when sintering temperatures were in the range 1000–1200 °C. The bulk ceramics (Co)_x(Ga₂O₃)_{0.6-x}(ZnS/Se)_{0.4} show a promising potential for future applications.

Received 4th July 2017
Accepted 18th October 2017

DOI: 10.1039/c7ra07354b

rsc.li/rsc-advances

1. Introduction

Group II–VI and III–V transition metal (TM) doped chalcogenide materials, especially ZnS and ZnSe crystals, have received extensive attention over the years because of their faster optical response time, wider transparency range in the mid-infrared, low optical loss, low phonon energy, high linear or nonlinear refractive index, good chemical stability and unique photosensitive properties, which are widely used in sensors, optical thin films and absorption in the mid-infrared region.^{1–8} Co has abundant absorption and emission energy levels and ferromagnetism, which makes it attractive among other transition metals. In addition, the semiconductor oxide Ga₂O₃ has a large energy gap of 4.9 eV for its direct band-gap, which is very suitable for emission, or to stimulate the spectrum of ultraviolet, visible and near infrared. Therefore, many researchers are focused on the preparation and relevant properties of these materials such as Co doped in ZnS,^{9–11} Ga doped in ZnSe,^{12–14} Co–Ga co-doped in ZnO,¹⁵ Co–Fe co-doped in ZnS/Se,¹⁶ Ga–Mn co-doped in ZnO,¹⁷ and the diluted magnetic semiconductors ZnCoO.^{18,19} But, most of the previous work was concerned with thin films, crystals, quantum dots, nano-wires or nano-particles, and less so with the bulk material. There are still many unsolved problems with these materials, such as the quality of raw material, the growth conditions and the impact of the dopant. In fact, bulk ceramics are also valuable

materials for research, to understand the relationship between the bulk and thin films or other nano-materials. Furthermore, the effect of the different performance of the bulk and the optimization strategies should be discussed. Recently, various techniques have been used to prepare films such as pulsed laser deposition (PLD),²⁰ molecular beam epitaxy (MBE),²¹ and metal organic chemical vapor deposition (MOCVD).²² In short, it is important to fabricate high quality raw materials and thin films.

In this paper, a material with Co–Ga₂O₃ co-doped in bulk ceramic ZnS/Se, (Co)_x(Ga₂O₃)_{0.6-x}(ZnS/Se)_{0.4} ($x = 0.1, 0.3$ and 0.5) is reported for the first time; the material was prepared *via* a solid state reaction in a high temperature pipe boiler. The influence of the temperature on the preparation, structure and spectral characteristics was investigated for the (Co)_x(Ga₂O₃)_{0.6-x}(ZnS/Se)_{0.4} bulk ceramic. The main motivations of our paper can be summarized in two points: investigating the relationship between the preparation of target or bulk ceramics and the future characteristics of the film, and acquiring the optimum preparation methods to achieve excellent doping in the material. Our research will be an important reference for related research areas.

2. Experimental

The (Co)_x(Ga₂O₃)_{0.6-x}(ZnS/Se)_{0.4} bulk ceramics were prepared *via* a solid state reaction in a high temperature pipe boiler. The raw ceramic bulk ZnS (99.99%), Co (99.99%) and Ga₂O₃ (99.999%) powders were weighed using an electronic balance according to the stoichiometric values. The powder was

College of Applied Sciences, Beijing University of Technology, Beijing, 100124, China.
E-mail: lwang.1@bjut.edu.cn; Tel: +86-10-67392198

manually ground for about 2 h in an agate mortar, and mechanically ball-milled for about 6 h three times, with respect to the degree of their mixed and granular size. The mixed powder was pressed in a $\Phi 20$ mm cylindrical mould under 10 MPa pressure for 15 min and then the preparation of the cylindrical bulk material was complete. The bulk was put in a tube furnace at 800–1400 °C for 6–10 h. The process described above was used to make all six stoichiometric $(\text{Co})_x(\text{Ga}_2\text{O}_3)_{0.6-x}(\text{ZnS/Se})_{0.4}$ materials. Also, an Ar atmosphere was pumped into the high temperature pipe boiler, eliminating the effect of oxygen in sintering.

The mass loss and size shrinkage rate of the bulk materials were recorded before and after sintering, and the relationship between the sintering temperature, mass loss and size shrinkage rate was calculated. The change of constituents in the bulk materials was measured by an X-ray fluorescence spectrometer (PANalytical Magix PW2403). The structures of the $(\text{Co})_x(\text{Ga}_2\text{O}_3)_{0.6-x}(\text{ZnS/Se})_{0.4}$ bulk ceramics were analyzed by XRD (BRUKER D8 ADVANCE), and Raman spectroscopy (Horiba Jobin Yvon T6400 spectrograph) at an excitation wavelength of 325 nm. The optical properties of the bulk ceramics were examined by UV-vis and near-infrared absorption spectroscopy using a U-4100 spectrometer. The valence state of Co and Ga was tested by XPS (X-ray photoelectron spectroscopy using Escalab 250 Thermo). The surface morphology of the thin film was imaged by SEM (JEOLJSM 6500F).

3. Results and discussion

3.1. The effect of sintering temperature

The mass loss rate of the $(\text{Co})_x(\text{Ga}_2\text{O}_3)_{0.6-x}(\text{ZnS/Se})_{0.4}$ ceramic bulk depends on the sintering temperature, ranging from 800 °C to 1400 °C, as shown in Fig. 1. The quality of the material changed to some extent before and after sintering. The raw material powder became the target ceramic by a process of weighing, grinding, ball-milling, pressing and sintering. The mass loss rate is calculated by the following formula:

$$\eta_m = \frac{M_1}{M_2} \times 100\% \quad (1)$$

where η_m is the mass loss rate of the sample, and M_1 and M_2 are the mass of sample before and after sintering, respectively. Research on the mass loss rate was employed to investigate the change in the constituents of the materials. Four sintering temperatures, 800, 1000, 1200 and 1400 °C, are used in this paper to investigate the relationship between the mass and temperature. In Fig. 1, the overall trend of the six different stoichiometric $(\text{Co})_x(\text{Ga}_2\text{O}_3)_{0.6-x}(\text{ZnS/Se})_{0.4}$ bulk ceramics shows an increase in the mass loss rate when the temperature rises. It is a fact that all of the materials with ZnS, rather than ZnSe, have sharply improved after 1200 °C, which illustrates that the loss rate increased especially in the bulks with ZnS. Whereas Ga is not stable enough to restrain the formation of the Ga–O bond. ZnS has a higher loss rate than ZnSe because ZnS is more likely to produce sulfide (SO_2 , SO_3) at high temperatures. Another reason for the enhancement of the ZnS loss rate is that the absorption properties of the two doped elements in ZnS are weaker than in ZnSe. What's more, the loss rate of the three stoichiometric ZnSe ceramics being lower than that of the ZnS ceramics also indicates that ZnSe has better absorption properties for the two kinds of doped-elements, a completely solid reaction and stable bonds. In summary, the mass loss rate of the ceramic bulks reached a maximum at 1400 °C and a minimum at 800 °C, rising slightly in the range of 1000–1200 °C. The mass loss rate of the three stoichiometric ZnSe ceramics was relatively stable in the range of 800–1200 °C, increasing by 0.5 percent.

The relationship between sintering temperature and molar ratio of the $(\text{Co})_x(\text{Ga}_2\text{O}_3)_{0.6-x}(\text{ZnS/Se})_{0.4}$ ceramic bulks is shown in Fig. 2. The variation of the ratio between the components in the material is obtained from the graph, which shows ZnS/Se, $\text{ZnCoGa}_2\text{O}_4$, Co and Ga_2O_3 . In general, the molar ratio of ZnS decreases, while the molar ratio of Ga_2O_3 increases. Co and $\text{ZnCoGa}_2\text{O}_4$ exhibit a trend of decline with the reduction of Co content and rise of Ga_2O_3 content, confirming the rule and analysis of Fig. 1. From Fig. 2(a), the molar ratio of ZnS is quite a bit higher than the Co content and the molar ratio of Co is reduced by about 30%. This demonstrates that Co has been doped into ZnS and obtained a better absorbing power in the chalcogenide. What's more, the content of each component is stabilized in the range 800–1200 °C, when the stoichiometric ratio has a higher doping of Co and lower doping of Ga_2O_3 , namely $(\text{Co})_x(\text{Ga}_2\text{O}_3)_{0.6-x}(\text{ZnS/Se})_{0.4}$. From Fig. 2(b) we find that the content of Ga_2O_3 has elevated dramatically and that of ZnS has decreased to a nearly normal mixing ratio, which explains the absorption efficiency of Co dropping with the rise of the doping content of Ga_2O_3 . The content of each component remains stable in the range 1000–1200 °C. Fig. 2(c) shows that the molar ratio of Co is relatively low because of the higher absorption and lower doping concentration of Co ions in the $(\text{Co})_{0.5}(\text{Ga}_2\text{O}_3)_{0.1}(\text{ZnS/Se})_{0.4}$ ceramic. In addition, the content of $\text{ZnCoGa}_2\text{O}_4$ is reduced by the change in Co concentration. An important effect with the change of Ga content in our materials was also confirmed by this result. The content of each component remains stable in the range 1000–1200 °C.

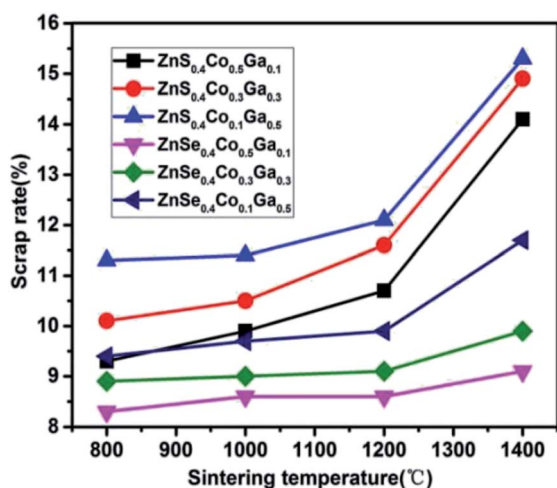


Fig. 1 The mass loss rate dependence on the sintering temperature.



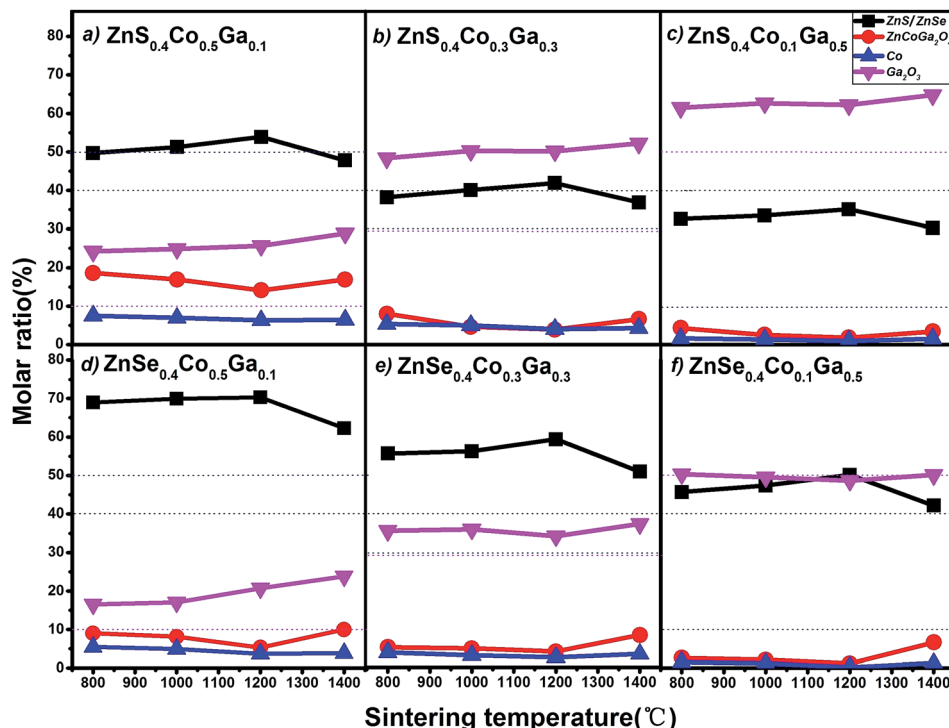


Fig. 2 The relationship between the sintering temperature and molar ratio of $(\text{Co})_x(\text{Ga}_2\text{O}_3)_{0.6-x}(\text{ZnS/Se})_{0.4}$. (a), (b) and (c) show the content and proportion of each component in $(\text{Co})_x(\text{Ga}_2\text{O}_3)_{0.6-x}(\text{ZnS})_{0.4}$. (d), (e) and (f) show the content and proportion of each component in $(\text{Co})_x(\text{Ga}_2\text{O}_3)_{0.6-x}(\text{ZnSe})_{0.4}$. The dotted lines in the figure represent the normal mixing ratio.

Fig. 2(d) shows a high molar ratio of ZnSe when the stoichiometric ratio has a higher doping of Co and lower doping of Ga_2O_3 and $(\text{Co})_{0.5}(\text{Ga}_2\text{O}_3)_{0.1}(\text{ZnS/Se})_{0.4}$. This situation indicates that ZnSe has a higher absorption than ZnS in terms of the Co element in the chalcogenide, which is reflected by the fact that the content of each component remains stable in the range 800–1000 °C. The trend, similar to that of ZnS above, is shown in Fig. 2(e), but the rate and range of the descent of the molar ratio of ZnSe are higher than ZnS in the same conditions and stoichiometry. This fact proves that the absorption properties of ZnSe are higher than those of ZnS in terms of doping ions. Besides, the increased stability also is reflected by the graph in the range 800–1000 °C. Fig. 2(f) shows a similar law to that of ZnS, and the content of each component remains stable in the range 1000–1200 °C.

In summary, all of the samples have a minimum content of $\text{ZnCoGa}_2\text{O}_4$ at 1200 °C and the best performance in the range 800–1200 °C. Furthermore, all of the samples have the lowest loss rate at 800 °C according to Fig. 1, but each of the stoichiometries has the highest content of $\text{ZnCoGa}_2\text{O}_4$ at 800 °C. Therefore, we conclude that the optimum sintering temperature range for this material is 1000–1200 °C. The absorption rate of Co ions for ZnSe is higher than that for ZnS. The best doping proportion is $x = 0.5$.

The relevance of the sintering temperature and shrinkage rate of the $(\text{Co})_x(\text{Ga}_2\text{O}_3)_{0.6-x}(\text{ZnS/Se})_{0.4}$ ceramic bulk is shown in Fig. 3. The shrinkage rate is calculated by the difference in the diameter of the sample before and after sintering. The loss rate

can be affected by a change of the molar ratio in a material. The change in the loss rate can directly lead to deformation of the material, which may further result in a transformation of the structure, stress and density of $(\text{Co})_x(\text{Ga}_2\text{O}_3)_{0.6-x}(\text{ZnS/Se})_{0.4}$. Therefore, practical significance was endowed upon the investigation of the relationship between the sintering temperature and shrinkage rate. Meanwhile, investigations can also be used to verify the range of the optimum sintering temperature in $(\text{Co})_x(\text{Ga}_2\text{O}_3)_{0.6-x}(\text{ZnS/Se})_{0.4}$. As the experiment used a 20.0 mm

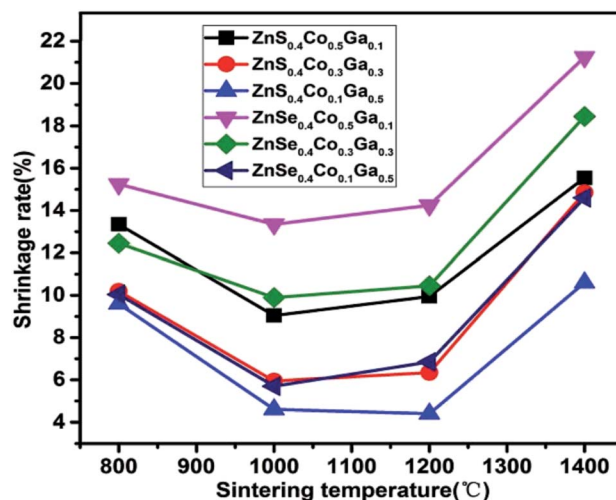


Fig. 3 The shrinkage rate with different sintering temperatures.



cylindrical mould in the preparation, the diameter of all samples can be regarded as 20.0 mm before sintering. Fig. 3 shows that all six materials show the same trend that increases after an initial decrease. But, in general, the shrinkage rate of ZnSe is higher than that of ZnS, which conforms with the relationship between the sintering temperature and molar ratio, and further explains the reason why the absorptivity of ZnSe is higher than that of ZnS. All of the samples have the lowest shrinkage rate in the range 1000–1200 °C, which directly proved the conclusions above. It is concluded that the shrinkage of the material is smallest in the range 1000–1200 °C.

3.2. The analysis of structure

The XRD patterns of the $(\text{Co})_x(\text{Ga}_2\text{O}_3)_{0.6-x}(\text{ZnS/Se})_{0.4}$ ceramic bulks sintered at 1200 °C are shown in Fig. 4. The acquired patterns were compared with standard library cards in the JCPDS database, including ZnS (JCPDS 65-9583), ZnSe (JCPDS 37-1463), α -Co (JCPDS 89-4307) and Ga_2O_3 (JCPDS 43-1012). The result demonstrates that all of the samples are cubic phase and there is no single phase of Co, Ga_2O_3 with Co high-doped and Ga_2O_3 low-doped in $(\text{Co})_{0.5}(\text{Ga}_2\text{O}_3)_{0.1}(\text{ZnS/Se})_{0.4}$, which suggests that multi-phase materials didn't exist in the initial state of the powder. Furthermore, a more complete solid phase reaction is found under the condition of a $(\text{Co})_{0.5}(\text{Ga}_2\text{O}_3)_{0.1}(\text{ZnS/Se})_{0.4}$ doping ratio.

$\text{ZnCoGa}_2\text{O}_4$ was found in the XRD pattern of the $(\text{Co})_x(\text{Ga}_2\text{O}_3)_{0.6-x}(\text{ZnS/Se})_{0.4}$ ceramic bulks as the content of Ga_2O_3 increased and Co decreased. This is a result of a more fully solid-phase reaction in the powders of Co, Ga_2O_3 and ZnS with the rise of Ga_2O_3 in high sintering temperature conditions. Oxygen replaced sulphur in the reaction, but elemental sulphur didn't appear in the XRD pattern, which suggests that sulphur still existed in the ZnS (similar to ZnSe). Most importantly, the replacement didn't destroy structure of the ZnS and ZnSe. Besides, the diffraction peaks of Ga_2O_3 were found in the XRD pattern with the rise of Ga_2O_3 content, which illustrates that the absorptivity of ZnS/Se for Ga_2O_3 is limited. The fact has a certain

relationship with the stability of Ga_2O_3 .²³ It is inevitable that the material is formed *via* solid-phase sintering.^{24,25} In conclusion, the XRD patterns of ZnSe show that it has better structural properties than ZnS due to the absorptivity and doping efficiency. Higher doping of Co and lower doping of Ga_2O_3 (namely $x = 0.5$) are regarded as the best doping proportions.

The Raman spectra of the $(\text{Co})_x(\text{Ga}_2\text{O}_3)_{0.6-x}(\text{ZnS/Se})_{0.4}$ ceramic bulks sintered at 1200 °C are shown in Fig. 5. There is no phonon signal corresponding to wurtzite of ZnS or ZnSe.²⁶ The Raman peaks of ZnS at 312.5 and 197.6 cm^{-1} , and ZnSe at 236.6 and 176.4 cm^{-1} in the spectra can be explained by the LO and TO phonon modes.^{27,28} The vibrations of the Ga_2O_3 structure are shown by the peak at 336.1 cm^{-1} ,²⁹ and the peaks at 414.8, 653.7 and 762.4 cm^{-1} are the vibrations of the Ga–O, Zn–O and Ga–O bonds.^{30,31} But, the Raman peak at 336.1 cm^{-1} doesn't exist in ZnSe with the same stoichiometry. The peaks in the Raman spectra at 464.7, 652.3 and 860.7 cm^{-1} for ZnSe can be attributed to Ga–O, Zn–O and Ga–O bonds.^{31,32} Although the two kinds of materials are relatively similar in their structure, the difference in absorptivity of Ga is well reflected in the research of the ZnS and ZnSe ceramic bulks. Meanwhile, there is no relevant information on Co in the Raman spectra, but there is in the results of XRD, which illustrates that the two materials have a similar ability to absorb Co and Co has a better absorption in the bulk of the materials. In addition, the two kinds of materials have the same trend in the change of stoichiometry, and the best doping proportion is a higher doping of Co and a lower doping of Ga_2O_3 in the same content of ZnS/ZnSe.

3.3. The properties of absorption

The UV-vis absorption spectra of the $(\text{Co})_x(\text{Ga}_2\text{O}_3)_{0.6-x}(\text{ZnS/Se})_{0.4}$ ceramic bulks sintered at 1200 °C are shown in Fig. 6. There is

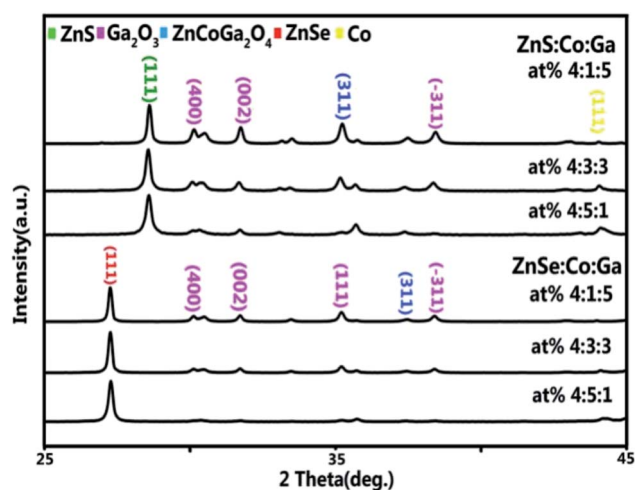


Fig. 4 XRD patterns of the $(\text{Co})_x(\text{Ga}_2\text{O}_3)_{0.6-x}(\text{ZnS/Se})_{0.4}$ ceramic bulks.

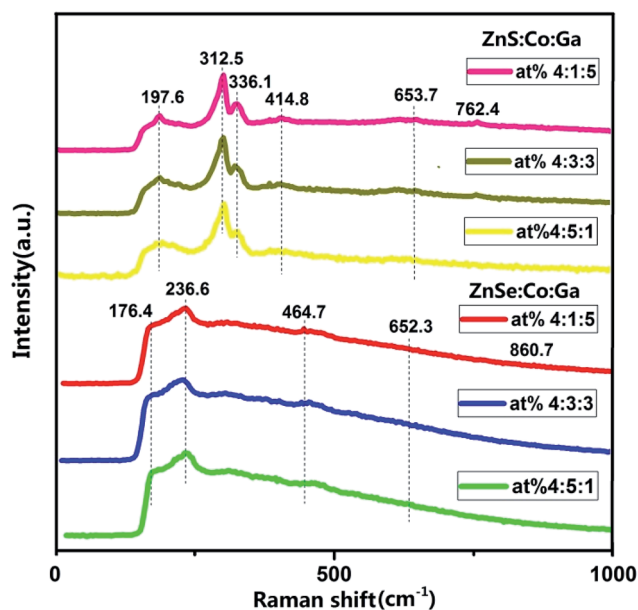


Fig. 5 Raman spectra of the $(\text{Co})_x(\text{Ga}_2\text{O}_3)_{0.6-x}(\text{ZnS/Se})_{0.4}$ ceramic bulks.



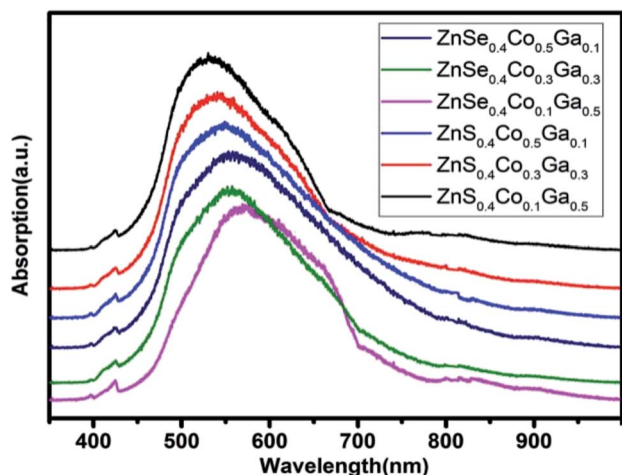


Fig. 6 UV-vis absorption spectra of the $(\text{Co})_x(\text{Ga}_2\text{O}_3)_{0.6-x}(\text{ZnS/Se})_{0.4}$ bulks.

a wide absorption band in the range 450–700 nm. The center of the peak is located in the range 540–570 nm. The absorption intensity is increased with the content of Ga_2O_3 , proving that Ga_2O_3 and Ga^+ have been doped in the ZnS/ZnSe because of its properties in the ultraviolet region.³³ The absorption peaks in the range 420–435 nm can be attributed to oxides in the bulks, and the intensity of the peaks shows little change.³⁴ Therefore, information about Ga_2O_3 and $\text{ZnCoGa}_2\text{O}_4$ is demonstrated in the absorption spectra. In order to verify the substitution of Co in the ceramic bulks, infrared spectroscopy will be used.

The infrared absorption spectra of the $(\text{Co})_x(\text{Ga}_2\text{O}_3)_{0.6-x}(\text{ZnS/Se})_{0.4}$ ceramic bulks sintered at 1200 °C are shown in Fig. 7. According to current reports, Co^{2+} has two strong absorption bands at 730 nm and 1600 nm, which are ascribed to $4\text{A}_2(\text{F}) \rightarrow 4\text{T}_1(\text{F})$ and $4\text{A}_2(\text{F}) \rightarrow 4\text{T}_1(\text{P})$.^{16,35} In the case of co-doped materials, the excited state $4\text{T}_1(\text{F})$ may lead to an energy transition between the relevant orbitals of the different

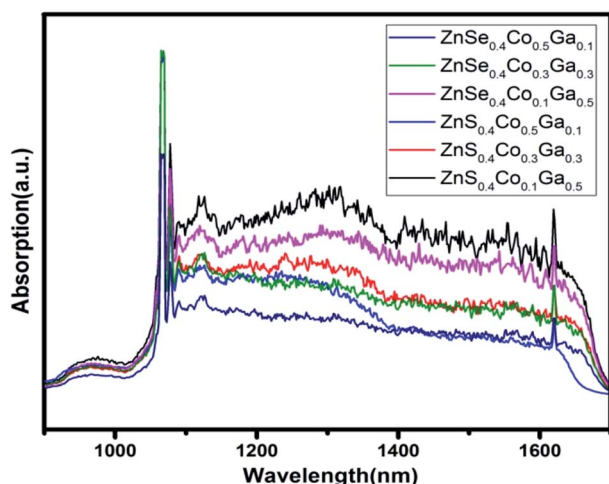


Fig. 7 Near-infrared absorption spectra of the $(\text{Co})_x(\text{Ga}_2\text{O}_3)_{0.6-x}(\text{ZnS/Se})_{0.4}$ bulks.

doping ions.³⁶ Therefore, the different dopants need to be tested and studied in different substrates. The infrared absorption spectra have two larger peaks approximately at 1080 nm and 1620 nm, which can be attributed to the oxide and d-d electronic transitions of the Co^{2+} ions. The intensity of the infrared absorption peaks depends on the molecular vibration with the change of dipole moment.³⁷ With Co^{2+} ion doping, the variation of the dipole moment becomes smaller. However, the infrared absorption band becomes narrow and sharp in the case of Ga_2O_3 doping.

3.4. The properties of the valence state

The XPS spectra of Co in the $(\text{Co})_x(\text{Ga}_2\text{O}_3)_{0.6-x}(\text{ZnSe})_{0.4}$ ceramic bulk are shown in Fig. 8. The C 1s in elemental C and Al targets is selected to revise the charge potential shift and bombardment in testing. The weak XPS signals at 800 °C are difficult to analyse, which indicates the uncertainty of Co doping at low temperatures. The binding energy of $\text{Co } 2\text{p}_{3/2}$ is 781.4 eV and $\text{Co } 2\text{p}_{1/2}$ is 797.7 eV in the range 1000–1200 °C. Compared with the standard spectrum, the peak information in this area coincides with the peak phase of CoO. Therefore, this situation proves the +2 valence of Co. With the increase of the preparation temperature, the peak position in the range 1200–1400 °C moves slightly in the direction of the 770 eV. The peak position is close to that of Co_3O_4 , according to information from standard spectra. This means that a small amount of Co ions with a +3 valence exist in the material sintered at high temperature.

The XPS spectra of Ga in the $(\text{Co})_x(\text{Ga}_2\text{O}_3)_{0.6-x}(\text{ZnSe})_{0.4}$ ceramic bulk are shown in Fig. 9. The peak positions of Ga 2p for the materials prepared at different temperatures are almost identical. The binding energy of $\text{Ga } 2\text{p}_{3/2}$ is 1117.8 eV and $\text{Ga } 2\text{p}_{1/2}$ is 1145.5 eV. This result shows that the influence of the sintering temperature on Ga is smaller than that on Co. In addition, this is also related to the high stability of Ga_2O_3 . According to the bonding energy of the Ga–O bond (1116.6 eV), we can conclude that Ga exists in the +3 oxidation state, and it is

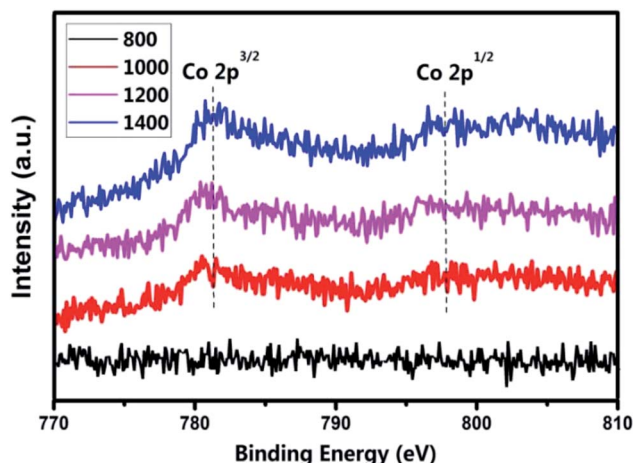


Fig. 8 XPS spectra of Co 2p for the $(\text{Co})_{0.5}(\text{Ga}_2\text{O}_3)_{0.1}(\text{ZnSe})_{0.4}$ bulks at temperatures ranging from 800 °C to 1400 °C.



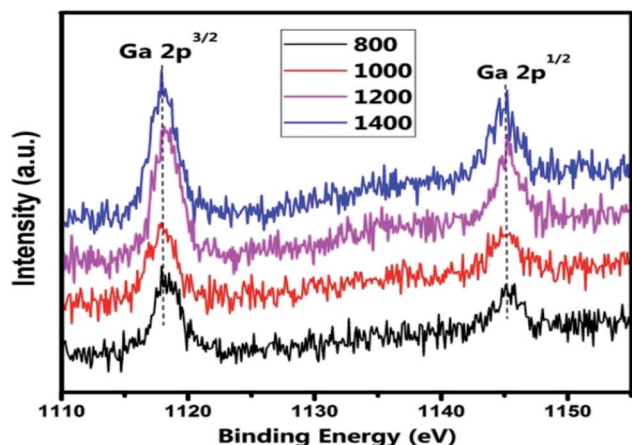


Fig. 9 XPS spectra of Ga 2p for the $(\text{Co})_{0.5}(\text{Ga}_2\text{O}_3)_{0.1}(\text{ZnSe})_{0.4}$ bulks at temperatures ranging from 800 °C to 1400 °C.

consistent with the Ga_2O_3 we doped. Therefore, the +3 valence of Ga ion is confirmed.

3.5. The surface morphology of the films

SEM used to visualise the surface morphology of $(\text{Co})_{0.5}(\text{Ga}_2\text{O}_3)_{0.1}(\text{ZnSe})_{0.4}$ films, prepared from the bulk sintered at 800 °C, 1000 °C, 1200 °C and 1400 °C, is shown in Fig. 10. Many incomplete dopant sites are present in the morphology at 800 °C, as shown in Fig. 10(a), which are probably Co sites because Co occupies 50% of the composition ratio at this doping concentration. The large particle size and surface roughness are shown in Fig. 10. However, the surface

morphology of the film prepared from the ceramic bulk sintered at 1000 °C has significantly improved, as depicted in Fig. 10(b). The number and size of the surface particles are markedly reduced by the change in temperature. At the same time, the neat surface arrangement and clear texture are depicted in Fig. 10(b). Then, the arrangement of the surface is almost unchanged, but the particle size is slightly increased for the film prepared from the ceramic bulk sintered at 1200 °C, as shown in Fig. 10(c). Although the surface is more smooth and uniform, some flaky dopant appears on the surface of the film sintered at 1400 °C. In summary, excellent surface morphology of the film is obtained in the range 1000–1200 °C. According to the results of this paper, this conclusion can be considered as an influence of the quality of the original material. The effect of the surface morphology of the raw material on the morphology of the film requires further discussion and experiment.

4. Conclusion

The ceramic bulks $(\text{Co})_x(\text{Ga}_2\text{O}_3)_{0.6-x}(\text{ZnS/Se})_{0.4}$ ($x = 0.1, 0.3$ and 0.5) were fabricated *via* a solid state reaction in a high temperature pipe boiler, at temperatures ranging from 1000 to 1400 °C. The impressive effect of the sintering temperature on the doping elements was investigated, and the optimum sintering temperature in the range 1000–1200 °C was revealed, by the analysis of the mass loss, molar ratio and shrinkage rate of $(\text{Co})_x(\text{Ga}_2\text{O}_3)_{0.6-x}(\text{ZnS/Se})_{0.4}$. The zinc-blende structure of the bulk ceramic and optimum doping ratio of $(\text{Co})_x(\text{Ga}_2\text{O}_3)_{0.6-x}(\text{ZnS/Se})_{0.4}$ were confirmed by XRD and Raman spectroscopy. $(\text{Co})_x(\text{Ga}_2\text{O}_3)_{0.6-x}(\text{ZnS/Se})_{0.4}$ could be used as an optical material with a broad application range, from the ultraviolet to infrared,

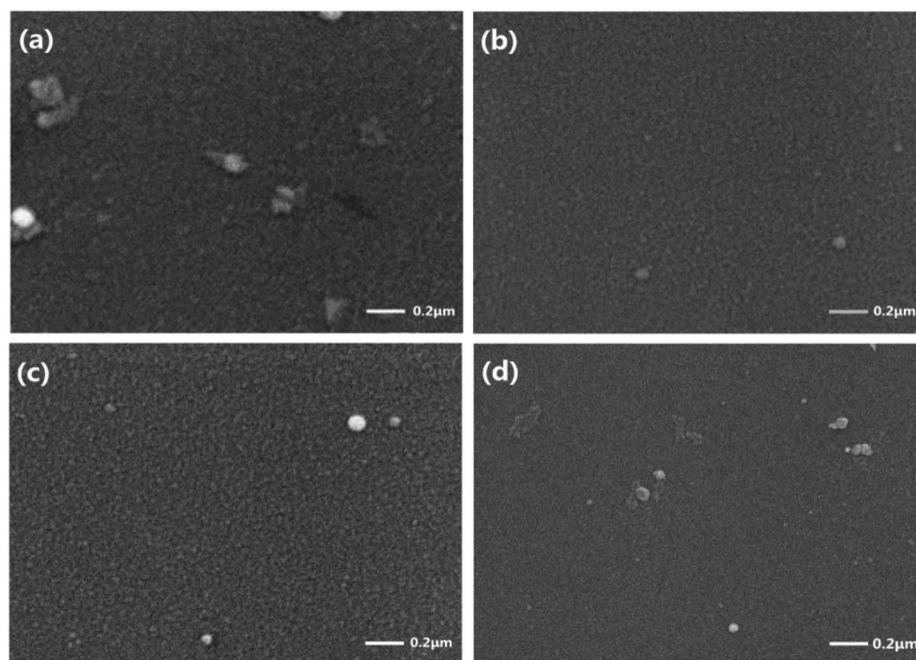


Fig. 10 SEM used to visualise the surface morphology of $(\text{Co})_{0.5}(\text{Ga}_2\text{O}_3)_{0.1}(\text{ZnSe})_{0.4}$ films prepared from the bulk sintered at (a) 800 °C, (b) 1000 °C, (c) 1200 °C and (d) 1400 °C.



according to the absorption spectra. The +2 and +3 valences of Co and Ga in the materials were proved by XPS. The surface morphologies of the films were visualised by SEM and exhibited excellence when sintering temperatures were in the range 1000–1200 °C. In summary, Co and Ga₂O₃ co-doped ZnS/Se ceramics have diverse properties and a wide range of absorption. What's more, it is beneficial to research the relationship between the preparation of target or bulk ceramics and the characteristics of the nano-materials. But, there are still some problems with our experiments, such as optimization for the preparation method and impurity in the materials. Therefore, this work is of great practical significance for investigations on bulk ceramics.

Conflicts of interest

There are no conflicts to declare.

Acknowledgements

This research is supported by the Beijing Municipal Education Commission Science and Technology Program key projects: KZ201610005001.

References

- 1 M. Gruning and C. Attacalite, *Phys. Chem. Chem. Phys.*, 2016, **18**, 21179–21189.
- 2 Q. Mahmood, S. M. Alay-e-Abbas, M. Hassan and N. A. Noor, *J. Alloys Compd.*, 2016, **688**, 899–907.
- 3 T. Y. Tsai and M. Birnbaum, *J. Appl. Phys.*, 2000, **87**, 25.
- 4 A. S. Hassanien, K. A. Aly and A. A. Akl, *J. Alloys Compd.*, 2016, **685**, 733–742.
- 5 K. Pushpendra, J. Singh, M. K. Pandey, C. E. Jeyanthi, R. Siddheswaran, M. Paulraj, K. N. Hui and K. S. Hui, *Mater. Res. Bull.*, 2014, **49**, 144–150.
- 6 I. T. Zedan, A. A. Azab and E. M. El-Menyawy, *Spectrochim. Acta, Part A*, 2016, **154**, 171–176.
- 7 P. S. Hariharan, N. Subhanshini, J. Vasanthalakshmi and S. P. Anthony, *J. Lumin.*, 2016, **26**, 703–707.
- 8 G. C. Xing, W. Ji, Y. G. Zheng and Y. Ying, *Opt. Express*, 2008, **16**, 5715–5720.
- 9 L. Zhang, D. Z. Qin, G. R. Yang and Q. X. Zhang, *Chalcogenide Lett.*, 2012, **9**, 93–98.
- 10 L. Y. Liu, L. Yang, Y. T. Pu, D. Q. Xiao and J. G. Zhu, *Mater. Lett.*, 2012, **66**, 121–124.
- 11 M. Jadraque, A. B. Evtushenko, D. Ávila-Brandé, M. Lopez-Arias, V. Lorient, Y. G. Shukhov, L. S. Kibis, A. V. Bulgakov and M. Martin, *J. Phys. Chem. C*, 2013, **117**, 5416–5423.
- 12 M. Lei, X. L. Fu, H. J. Yang, Y. G. Wang, P. G. Li, Q. R. Hu and W. H. Tang, *Mater. Chem. Phys.*, 2012, **133**, 823–828.
- 13 Z. Mierczyk, A. Majchrowski, K. Ozga, A. Slezak and I. V. Kityk, *Opt. Laser Technol.*, 2006, **38**, 558–564.
- 14 F. Sakurai, K. Suto, J. Nishizawa, Y. Oyama, M. Motozawa and Y. Hara, *J. Electrochem. Soc.*, 2000, **147**, 747–750.
- 15 X. C. Liu, Z. Z. Chen, B. Y. Chen, E. W. Shi and D. Q. Liao, *J. Cryst. Growth*, 2010, **312**, 2871–2875.
- 16 N. Myoung, D. V. Martyshev, V. V. Fedorov and S. B. Mirov, *J. Lumin.*, 2013, **133**, 257–261.
- 17 K. P. Wu, S. L. Gu and S. M. Zhu, *Semicond. Sci. Technol.*, 2008, **33**, 345–348.
- 18 J. A. Sans, J. F. Sanchez-Royo, J. Pellicer-Porres, A. Segura, E. Guillotel, G. Martinez-Criado, J. Susini, A. Munoz-Paez and V. Lopez-Flores, *Superlattices Microstruct.*, 2007, **42**, 226–230.
- 19 S. J. Luo, C. B. Wang, X. Zhou, Q. Shen and L. M. Zhang, *J. Mater. Sci.: Mater. Electron.*, 2012, **23**, 1477–1484.
- 20 M. Jadraque, A. B. Evtushenko, D. A. Brande, M. Lopez-Arias, V. Lorient, Y. G. Shukhov, L. S. Kibis, A. V. Bulgakov and M. Martin, *J. Phys. Chem. C*, 2013, **117**, 5416–5423.
- 21 S. R. Zandbergen, R. Gibson, B. Amirsolaimani, S. Mehravar, P. Keiffer, A. Azarm and K. Kie, *Opt. Mater. Express*, 2017, **7**, 2102–2110.
- 22 K. S. Kim, H. W. Kim and C. M. Lee, *Mater. Sci. Eng., B*, 2003, **98**, 135–139.
- 23 D. Y. Guo, Z. P. Wu, P. G. Li, Y. H. An, H. Liu, X. C. Guo, H. Yan, G. F. Wang, C. L. Sun and L. H. Li, *Opt. Mater. Express*, 2014, **4**, 1067–1076.
- 24 J. B. Chen, L. Wang, X. Q. Su, L. Kong, G. Q. Liu and X. P. Zhang, *Opt. Express*, 2010, **18**, 1398–1405.
- 25 T. L. Phan, P. Zhang, D. S. Yang, N. X. Nghia and S. C. Yu, *J. Appl. Phys.*, 2011, **110**, 063912.
- 26 H. I. Abdulgafour, Z. Hassan, N. Al-Hardan and F. K. Yam, *Phys. B*, 2010, **405**, 2570–2572.
- 27 C. M. Lin, D. S. Chuu, T. J. Yang, W. C. Chou, J. A. Xu and E. Huang, *Phys. Rev. B: Condens. Matter Mater. Phys.*, 1997, **55**, 13641–13646.
- 28 C. S. Yang, C. S. Ro, W. C. Chou, C. M. Lin, D. S. Chuu, J. Hu, E. Huang and J. Xu, *J. Appl. Phys.*, 1999, **85**, 8092–8096.
- 29 S. Kumar, G. Sarau, C. Tessarek, M. Y. Bashouti, A. Hahnel, S. Christiansen and R. Singh, *J. Phys. D: Appl. Phys.*, 2014, **47**, 1–10.
- 30 Y. H. Gao, Y. Bando and T. Sato, *Appl. Phys. Lett.*, 2002, **81**, 2267–2269.
- 31 R. Rao, A. M. Rao, B. Xu, J. Dong, S. Sharma and M. K. Sunkara, *J. Appl. Phys.*, 2005, **98**, 094312.
- 32 D. Dohy, G. Lucazeau and A. Revcolevschi, *J. Solid State Chem.*, 1982, **45**, 180–192.
- 33 M. Choi and J. Son, *Curr. Appl. Phys.*, 2017, **17**, 713–716.
- 34 J. M. Pawlikowski, *Solid State Commun.*, 1985, **55**, 31–33.
- 35 M. Luo, N. C. Giles, U. N. Roy, Y. Cui and A. Burger, *J. Appl. Phys.*, 2005, **98**, 08350.
- 36 B. Amin and I. Ahmad, *J. Appl. Phys.*, 2009, **106**, 37101–37106.
- 37 X. S. Li, C. H. Li and W. Lin, *Phase analysis and research method of inorganic non-metallic materials*, China Building Material Industry Publishing House, Beijing, 2008, pp. 203–219.

